All-electrical driving and probing of dressed states in a single spin

Hong T. Bui[1,2‡], Christoph Wolf[1,3‡], Yu Wang[1,3], Masahiro Haze[4], Arzhang Ardavan[5], Andreas J. Heinrich[1,2], Soo-hyon Phark[1,3]**

[1]Center for Quantum Nanoscience, Institute for Basic Science (IBS), Seoul 03760, Korea

[2]Department of Physics, Ewha Womans University, Seoul 03760, Korea

[3]Ewha Womans University, Seoul 03760, Korea

[4]The Institute for Solid State Physics, University of Tokyo, Kashiwa 277-8581, Japan

[5]CAESR, Clarendon Laboratory, Department of Physics, University of Oxford, Oxford OX1 3PU, UK

ABSTRACT The sub-nanometer distance between tip and sample in a scanning tunneling microscope (STM) enables the application of very large electric fields with a strength as high as ~ 1 GV/m. This has allowed for efficient electrical driving of Rabi oscillations of a single spin on a surface at a moderate radio-frequency (RF) voltage of the order of tens of millivolts. Here, we demonstrate the creation of dressed states of a single electron spin localized in the STM tunnel junction by using resonant RF driving voltages. The read-out of these dressed states was achieved all-electrical by a weakly coupled probe spin. Our work highlights the strength of the atomic-scale

geometry inherent to the STM that facilitates creation and control of dressed states, which are promising for the design of atomic scale quantum devices using individual spins on surfaces.

KEYWORDS Dressed state, Electron spin resonance, Scanning tunneling microscopy, double electron-electron spin resonance, Autler-Townes doublets, Mollow Triplets

The creation of long-lived quantum states lies at the heart of understanding quantum-coherent phenomena and their application to practical problems such as quantum computing and quantum sensing [1]. The interaction of quantum states with the environment is critical for observing the quantum state, but also inevitably leads to the uncontrollable collapse of the wave function resulting in the loss of its quantum information in a process called decoherence [2]. In such open quantum systems, various strategies have been employed to improve the coherence of their quantum state. A particularly intriguing strategy is the creation of decoherence-free sub-spaces, which interact with the environment slowly compared to the dynamics of the quantum states, leading to a suppression of decoherence.

One feasible approach to such quantum states with long coherence times is to create so-called 'dressed states', which result from the coupling between the quantum spins and a coherent driving field, also known as the AC-Stark effect [3, 4]. This interaction transforms the eigenstates of the system from the non-interacting spin eigen basis into their superpositions, split by the coupling strength. The consequence is vacuum Rabi oscillations between the two states being dressed, as long as the coupling between spin and field is larger than the incoherent dynamics of the system, which contribute to the decay of Rabi oscillations [5]. In this case, the two levels are said to be

strongly driven and the spin eigenstates of the system are dressed with the resonant field (see also Supplementary 1). The dressed states can be probed by using an optical transition to a third level, where they appear as Autler-Townes doublets [3, 6] or Mollow Triplets [7, 8] in various two-level systems, such as cold atomic gasses [9-11], single molecules [12, 13], quantum dots [14, 15], and defects in semiconductor [4]. The driving field can be implemented over a wide range of energy, from lasers [16] to microwave [4, 17]. The STM tunnel junction with a characteristic gap of about one nanometer easily generates large electric fields on the order of ~ 1 GV/m, in contrast to centimeter-scale geometries common for similar experiments on bulk samples [18, 19]. Therefore, a spin confined in the STM junction can fall into the strong driving regime when driven by oscillating voltage of a moderate range, 0.01–1 V, which is easily accessible in normal operation conditions of an STM.

In this work, we demonstrate the creation and read-out of dressed states of single spins in a scanning tunneling microscope [20, 21]. We utilized a tailored atomic scale nanostructure of two weakly coupled electron spins (Fig. 1a), in which multi-spin control was achieved through a spin in the STM tunnel junction using the double resonance technique [22, 23]. Both spins were subjected to the applied radio frequency (RF) fields and selectively driven by tuning the RF frequency into resonance [24-28]. Resonant driving of one spin resulted in dressing of its states. Instead of using an optical transition to a third level, resonant transitions of the other spin were then used to probe the dressed states of the first spin in our experimental scheme, enabling both creation and read-out of the dressed states to be performed all-electrical with two RF voltages of moderate amplitude. Our scheme yielded Autler-Townes doublets as well as Mollow triplets in the double resonance spectra and, in addition, provided a direct way to measure the Rabi rates of both spins in a continuous-wave experiment.

Results and Discussion

We performed experiments on a designed nanostructure composed of two Ti atoms (each having electron spin of S = 1/2), hereafter referred to as Ti-1 and Ti-2, forming a pair of coupled electron spins. These spins were placed on a bilayer of MgO grown on a single crystalline Ag substrate (Fig. 1a) [29, 30]. The electron spin resonance (ESR) spectra of Ti-1 (Fig. 1b) and Ti-2 (Fig. 1c) were obtained by using continuous-wave single- and dual-frequency ESR, respectively[22]. From the spectra, we obtained the respective resonance frequencies of the coupled spins as well as the strength of their exchange interaction *J*. The eigenstates of this system can be well described by Zeeman product states $|S_z(\text{Ti-1})\ S_z(\text{Ti-2})\rangle$, yielding four possible transitions (with frequencies f_1 to f_4), which are addressable by tuning the frequency of the RF driving voltages, as depicted in Fig. 1d.

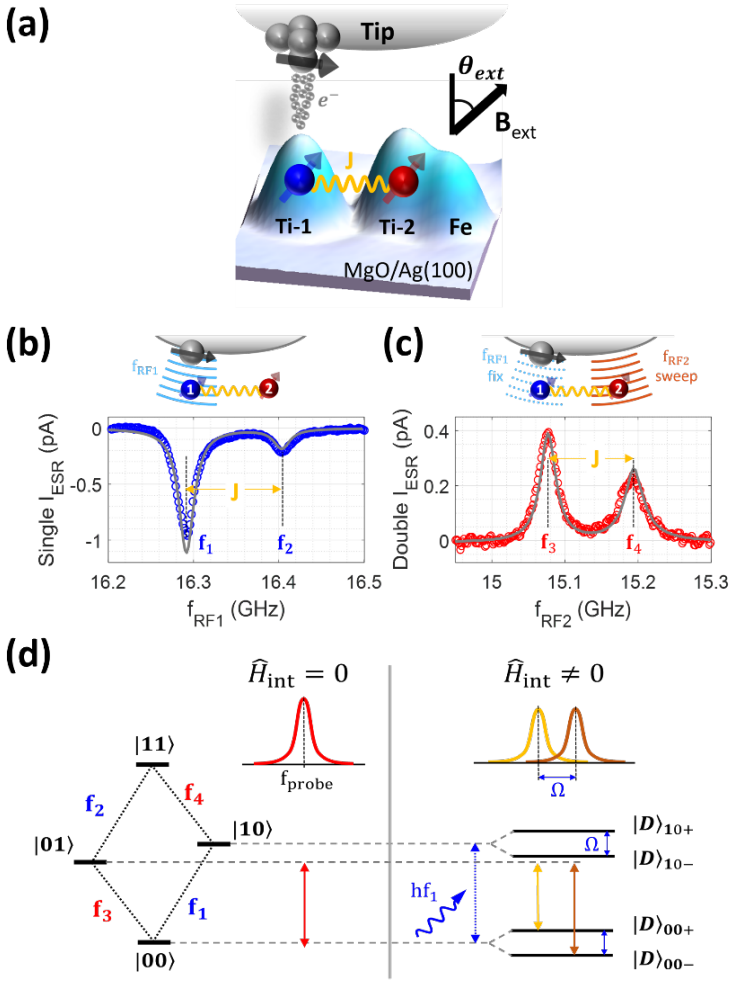

Figure 1. Dressing of a single spin in the STM tunnel junction by coupling with an oscillating field. (a) STM topographic image of an engineered nanostructure composed of two coupled spins: Ti-1 (in the tunnel junction), Ti-2 (outside the tunneling current), and one Fe adatom[31]. The Ti-1 to Ti-2 spacing is 1.22 nm, and Ti-2 to Fe is 0.59 nm ($I_{DC} = 10$ pA, $V_{DC} = 100$ mV) [22]. (b) and (c), Single and double resonance ESR spectra obtained from the structure in (a). In (b) the spectrum reveals two transitions of Ti-1 (labeled as f_1 and f_2), whilst in (c) the spectrum shows two transitions (f_3, f_4) of Ti-2 ($I_{DC} = 20$ pA, $V_{DC} = 50$ mV, $B_{ext} = 670$ mT, $\theta_{ext} = 60^{\circ}$, $V_{RF1} = 30$ mV; $V_{RF2} = 40$ mV for (c)). The grey curves are simulated spectra. The splitting of the peaks in each case

corresponds to the exchange coupling energy J between the two Ti spins. (d) Energy diagrams of two weakly coupled spins with four spin states labelled according to $|S_z(\text{Ti-1}), S_z(\text{Ti-2})\rangle$ and ESR transitions f_1, f_2, f_3, and f_4 corresponding to the four peaks shown in (b) and (c). Dressed-state picture of a quantum two level system, here for the first spin (Ti-1) for the cases of spin-field coupling OFF ($\widehat{H}_{\text{int}} = 0$) and ON ($\widehat{H}_{\text{int}} \neq 0$). The two relevant states ($|00\rangle$,$|10\rangle$) are dressed ($|D\rangle_{10\pm}, |D\rangle_{00\pm}$) when the coupling is switched ON. The transition f_3 is used to probe the dressed states.

Driving any of these four transitions close to their resonance frequency leads to dressing of the spin corresponding to the transition, which transforms the system eigenstates into the superposition of two relevant Zeeman product states of the undriven system. These eigenstates, called dressed states, are labeled as $|D\rangle$ in Fig. 1d. The energy splitting Δf between a pair of dressed states corresponds to the Rabi rate Ω, [32, 33] determined by the coupling strength between the two-level system and the driving field [3]. Our specific design of the double resonance measurement schemes [22] for a coupled spin system allows such dressed states to be spectroscopically probed by another transition to a state which does not undergo state dressing (i.e. $|01\rangle$ in Fig. 1d). To simultaneously dress and probe the spin states, we used two RF signal sources where we fixed the frequency of one RF voltage to dress one spin and swept the other across the resonances of the second spin to spectroscopically probe the dressed states as depicted schematically in Fig. 1d. All the spectra shown in Figs. 1–4 were obtained with the tip positioned on Ti-1.

We begin by dressing the Ti-1 spin and probing its splitting using a transition of Ti-2. In Fig. 2a, we show double resonance spectra obtained with varying RF voltage V_{RF1} with its frequency (f_{RF1}) fixed at a resonance of Ti-1 (f_1) and sweeping the frequency of the other RF voltage (f_{RF2})

across a resonance of Ti-2, f_3 (see Fig. 2b). Note that each spectrum was measured with the tip positioned on Ti-1, i.e., the spin-polarized tunneling current measures the ESR signal of the Ti-1 spin, which remained in resonance by the given V_{RF1} at f_1 during the frequency sweep of V_{RF2}. Our double resonance scheme is designed to read out zero intensity for the ESR signal of Ti-1 when Ti-2 is off-resonance, such that any non-zero intensity of a double resonance spectrum reflects a variation of the Ti-1 spin's resonance intensity in the frequency sweep of V_{RF2} [22]. Therefore, the peaks shown in Fig. 2a indicate a net reduction of the ESR signal of Ti-1 due to spin population transfer from $|00\rangle$ to $|01\rangle$, stemming from the resonance of the Ti-2 spin at $f_{\mathrm{RF2}} = f_3$. We note that the RF power induced local heating at the tunnel junction, which was read out by the sample temperature[22]. The temperature-induced modification of the spin populations of the four eigenstates, however, turned out to be negligible and has not been taken into account in this work (see Fig. S6).

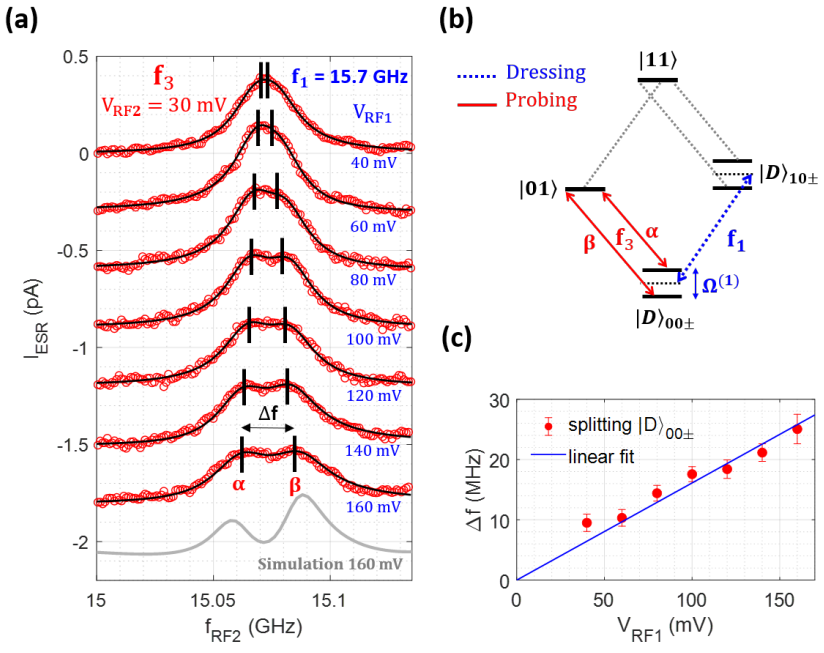

Figure 2. Double resonance spectroscopy on dressed states of Ti-1. (a) Double resonance spectra measured with RF2 frequency swept across an ESR transition (f_3) of Ti-2 and with RF1 frequency fixed at a resonance of Ti-1 ($I_{\mathrm{DC}} = 20$ pA, $V_{\mathrm{DC}} = 50$ mV, $V_{\mathrm{RF2}} = 30$ mV, $T = 0.4$ K, $B_{\mathrm{ext}} = 670$ mT, $\theta_{\mathrm{ext}} = 60^{\circ}$). An increasing driving amplitude of Ti-1 (V_{RF1}) led to an increased peak splitting (see α, β). The curves were fitted using two-peak Lorentzian function (solid black curves, also see detail in Fig. S2). The gray curve is a simulated spectrum using the experimental peak splitting as Rabi rate and spin relaxation times of $T_1^{(1)} = 8$ ns, $T_1^{(2)} = 150$ ns for the first and second spins, respectively. (b) A schematic energy level diagram illustrating the dressing of Ti-1 (f_1) and probing using Ti-2 (f_3). (c) Dependence of the splitting $\Delta f = \alpha - \beta$ on the driving amplitude V_{RF1} as obtained from the fitting of the spectra in (a). The solid line is a linear fit, giving the Rabi rate of the transition (f_1), $\Omega^{(1)}/V_{\mathrm{RF1}} = 0.16 \pm 0.015$ MHz/mV.

The formation of dressed states manifested as splitting of the double resonance peak, which increased monotonically for an increasing RF voltage V_{RF1}. The dressing of the Ti-1 spin, followed by the probing using Ti-2 transitions, is illustrated in Fig. 2b (also see Fig. S1). The two states $|00\rangle$ and $|10\rangle$ relevant to the transition f_1 are dressed, resulting in two eigenstates, $|D\rangle_{00\pm}$ and $|D\rangle_{10\pm}$, respectively. On driving the Ti-2 spin across f_3, the two dressed states stemming from $|00\rangle$ were probed as two resonant transitions α and β as depicted. We emphasize here that the Ti-2 spin probes the dressed states of the Ti-1 spin. The splitting Δf was visible when it was larger than the linewidths of the double resonance peaks and showed a linear dependence on V_{RF1}. From the linear fit in Fig. 2c we extracted the Rabi rate of the Ti-1 spin, $\Omega^{(1)}/(2\pi V_{\mathrm{RF1}}) = 0.160 \pm 0.015$ MHz/mV.

Next, we exchanged the roles of the two spins by dressing Ti-2 and probing with Ti-1. To achieve this in our double resonance experiment, we fixed f_{RF2} at the resonance f_3 of Ti-2 and swept f_{RF1} over the frequency range of the Ti-1 transitions. The resulting spectra are shown in Fig. 3a. When increasing the driving RF voltage V_{RF2}, we again observed splitting of the double resonance peaks. In contrast to the case in Fig. 2, the dressing of the Ti-2 spin at frequency f_3 splits the states, $|00\rangle$ and $|01\rangle$, into four dressed states, $|D\rangle_{00\pm}$ and $|D\rangle_{01\pm}$, respectively, as illustrated in Fig. 3b. Then, the dressed states were probed by the resonances f_1 and f_2 of Ti-1. The peak splitting Δf again showed a linear dependence on V_{RF2}, resulting in a Rabi rate of the Ti-2 spin, $\Omega^{(2)}/(2\pi V_{\mathrm{RF2}}) = 0.220 \pm 0.02\,\mathrm{MHz/mV}$ (Fig. 3c). Here, the Autler-Townes doublets in the double resonance spectroscopy allowed a direct measure of the strength of the remote driving of a spin outside of the tunnel junction as reported in our previous work [22, 23]. Note that the Rabi rate of the Ti-2 spin is comparable to that of the Ti-1 spin in the tunnel junction, demonstrating that our tailored quantum spin structure provides an effective way to remotely control the spins outside the STM tunnel junction.

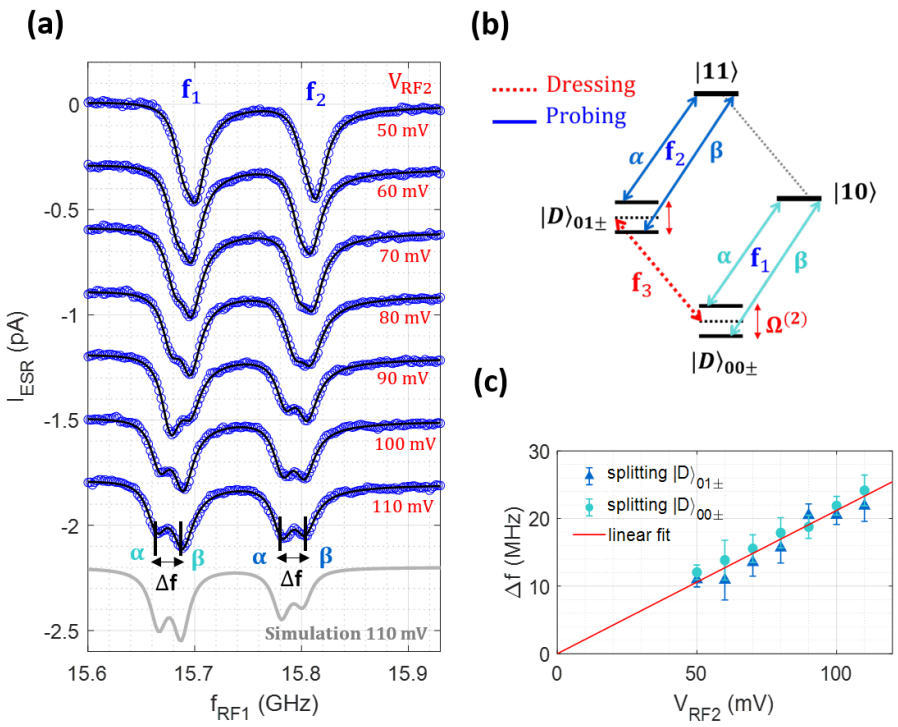

Figure 3. Double resonance spectroscopy on dressed states of Ti-2. (a) Double-resonance spectra measured with RF1 frequency swept across the ESR transitions (f_1, f_2) of Ti-1 and with RF2 frequency fixed at a resonance (f_3) of Ti-2 ($I_{\mathrm{DC}} = 20$ pA, $V_{\mathrm{DC}} = 50$ mV, $V_{\mathrm{RF1}} = 30$ mV, $T = 0.4$ K, $B_{\mathrm{ext}} = 660$ mT, $\theta_{\mathrm{ext}} = 70^{\circ}$; also see Fig. S4 for the four transition frequencies). An increasing driving amplitude of Ti-2 (V_{RF2}) led to an increased peak splitting (see α, β). The gray solid curve represents a simulated spectrum using the peak splitting as Rabi rate and spin relaxation times of $T_1^{(1)} = 8$ ns, $T_1^{(2)} = 150$ ns for the first and second spins, respectively. (b) A schematic energy level diagram illustrating the dressing of Ti-2 (f_3) and probing using Ti-1 (f_1, f_2). (c) Dependence of the splitting $\Delta f = \alpha - \beta$ on the driving amplitude V_{RF2} obtained from the fitting of the spectra in (a). The solid line is a linear fit, giving the Rabi rate of the transition (f_3), $\Omega^{(2)}/(2\pi V_{\mathrm{RF2}}) = 0.22 \pm 0.012$ MHz/mV.

We extended our double resonance scheme to observe the Mollow triplet [7, 8] from the dressed states of the Ti-2 spin. Here, we first measured a double resonance spectrum using the same scheme in Fig. 3b by driving only the transition f_3. As a result, the spectrum showed four peaks composed of two groups, where each group is the Autler-Townes doublet measured by the probing transition corresponding to either f_1 or f_2 (Fig. 4a). Then, we simultaneously drove both resonances (f_3 and f_4) of Ti-2 and measured the spectrum across the spin resonances of Ti-1. The resulting spectrum in Fig. 4b clearly shows six peaks composed of two groups, three peaks per group across each resonance of the Ti-1 spin. The simultaneous driving of both transitions f_3 and f_4 dressed all four states $|00\rangle$, $|01\rangle$, $|10\rangle$, $|11\rangle$, leading to four transitions (α', β', γ', δ') available when probed across each resonance of Ti-1, as illustrated in Fig. 4c. The transitions β' and γ' have the same frequency as the un-dressed states, whilst two others, α' and δ', are shifted by $-\Omega$ and $+\Omega$, respectively. This resulted in three peaks in each group, where the intensity of the central one is twice as large as those of the two side peaks, as seen clearly in the spectrum.

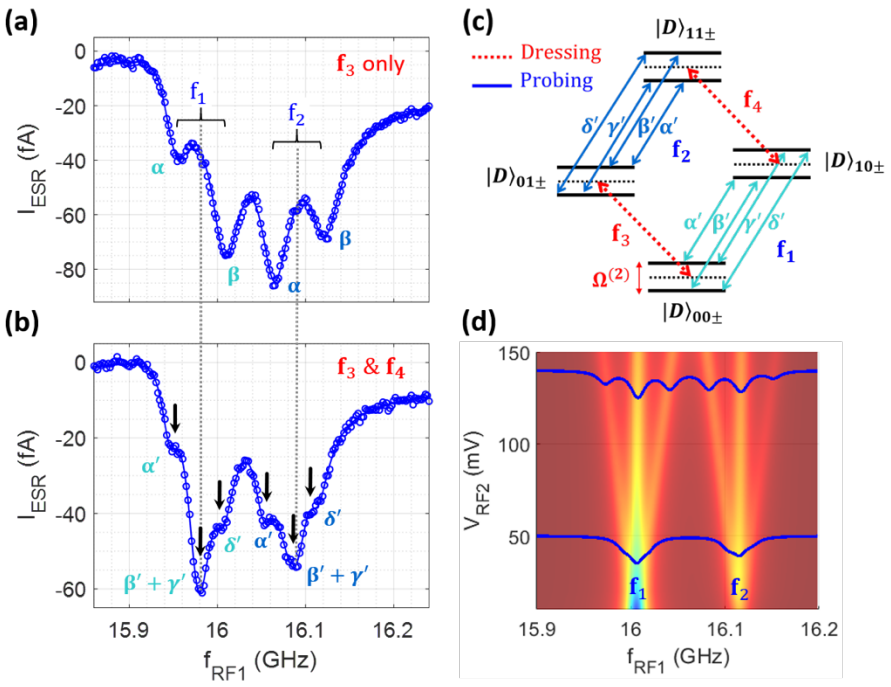

Figure 4. Mollow triplet from dressed states of Ti-2. (a) Double resonance spectra showing Autler-Townes doublets from the dressed states of Ti-2 at its transition f_3 with V_{RF2} = 120 mV and V_{RF1} = 20 mV. (b) Triple resonance spectra measured by applying V_{RF2} simultaneously on two transitions of Ti-2 (f_3 and f_4) with equal amplitudes, $V_{RF2}(f_3) = V_{RF2}(f_4) = 60$ mV, and on probing transitions (f_1 and f_2) V_{RF1} = 20 mV. Mollow triplets were observed (three peaks per probing transition), resulting from the 8 possible transitions across the probing transition frequencies, f_1 and f_2, as depicted in (c) ($I_{DC} = 20$ pA, $V_{DC} = 50$ mV, $T = 0.4$ K, $B_{ext} = 640$ mT, $\theta_{ext} = 65^{\circ}$; also see Fig. S4 for the four transition frequencies). The tip used in this measurement was different from the tip for Figs. 2 and 3. (c) Schematic of dressed states of Ti-2 under simultaneous driving of its two resonances f_3 and f_4. (d) Simulated Mollow triplet spectra vs. V_{RF2} amplitude, showing an increased splitting for an increasing V_{RF2}, with two representative spectra overlayed in blue.

We further implemented several control experiments to show the data reproducibility and study influence of measurement conditions on Rabi rates of both Ti-1 and Ti-2 spins (see Supplementary 2 and 3). First, we obtained the Autler-Townes doublets at different tip-atom distances, influencing the splitting of the doublets on Ti-2 ESR transitions (see Fig. S3). This is an evidence that the AC Stark effect is tunable using the tip-atom distance. Second, we observed the Autler-Townes doublets by dressing Ti-2 at various vector magnetic fields (Figs. S4A-C), which resulted in changes of Rabi rates (Figs. S4E-G). Third, we performed the same experiments using another spin-polarized tip and achieved Rabi rate at about twice the magnitude found from the data in Fig. 3 (Figs. S4D and H), which is attributed to the fact that different tip terminations can lead to different efficiencies in driving ESR.

To understand the spin dynamics of this work, we performed open quantum system simulations of two exchange-coupled spins using the Lindblad formalism with collapse operators to account for finite lifetime and coherence times of the spins (see also Supplementary 5) [34]. All the spectra of the Autler-Townes doublet were well reproduced by implementing double resonance spectroscopy schemes into the simulations and calculating the spin-polarized current using steady-state populations of the four quantum states (gray curves in Figs. 2 and 3). Our simulation using three RF driving voltages produced spectra also in quantitative agreement with the Mollow triplets in Fig. 4b (blue overlay spectrum at V_{RF2} = 50 mV) and estimated its driving-power dependence (Fig. 4d). Deviations in the relative peak heights are sensitive to detuning of the driving frequencies, which might stem from slight deviations of an experimental factor such as the fluctuation of the external magnetic field (see Fig. S7). We note that given our experimental

parameters the average number $\langle n \rangle$ of RF photons is large, and thus the resulting dressed states can be described using a semi-classical photon field (see Supplementary 1) [35-37].

Further insights into the state-dressing can be found by analyzing the time evolution of the density matrix elements. Our experimental scheme, using two coupled spins, differs from the conventional schemes by the all-electrical driving and readout of the dressed states [38]. This, however, turned out not to significantly influence the basic principle of state dressing, which was shown by tracing out the probe spin and analyzing the reduced density matrix only for the dressed spin $\rho^{(2)} = \mathrm{Tr}_1[\rho]$. Here, the indices 1 and 2 refer to probe and dressed spin, respectively. After tracing out the sensor spin, the resulting density matrix of the dressed spin, composed of two diagonal elements, ρ_{00} and ρ_{11}, corresponding to the populations of the $|0\rangle$ and $|1\rangle$ states, respectively, and two off-diagonal elements, ρ_{01} and ρ_{10}, correspond to the coherences of the dressed spin (see Supplementary 6 for details).

We compare in Figs. 5a and 5b two simulated density matrices of the dressed spin driven at two driving RF amplitudes V_{RF2} = 20 and 140 mV, respectively, where the probe spin was weakly driven in all simulations at a fixed V_{RF1} = 30 mV, which is the same as in the experiments. A weakly driven system (V_{RF2} = 20 mV; Fig. 5a) showed that its populations, ρ_{00} and ρ_{11}, just decay slowly towards the steady states, in which the population distribution was determined by the driving amplitude. In contrast, a strongly driven system (V_{RF2} = 140 mV; Fig. 5b) showed clear Rabi oscillations of the populations in the transient ($0 < t < 50$ ns), indicating that here the driving power fulfilled the condition for the strong driving regime, where the spin-field coupling was larger than the decoherence dynamics of the system. The populations also decayed in the long-

time limit, however, saturating to near-equal values for $|0\rangle$ and $|1\rangle$ states, which are close to the limit in the continuous wave ESR. All our simulations were implemented in the lab frame, leading to additional fast oscillations as shown in the insets in Figs. 5a and 5b.

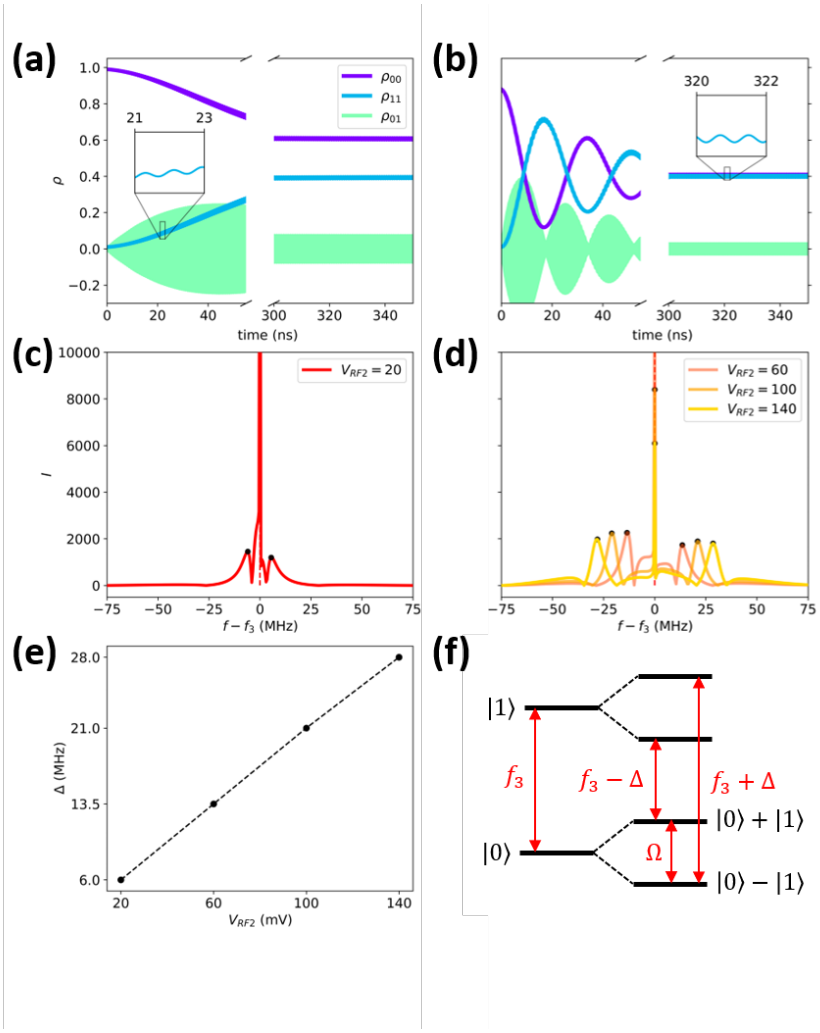

Figure 5. Dynamics of the dressed spin. Difference between the time-evolution of a weakly and strongly driven spin obtained from the reduced density matrix of the second spin (Ti-2). (a) time evolution of the diagonal elements, ρ_{00} and ρ_{11}, the populations of ground $|0\rangle$ and excited state $|1\rangle$ of a weakly driven (V_{RF2} = 20 mV) spin, respectively, reveals overdamped evolution of the populations towards the steady states. (b) in contrast, a strongly (V_{RF2} = 140 mV) driven spin shows

Rabi oscillations in the transient ($0 < t < 50$ ns) and near-equal populations in the long-time limit. (c) Fourier transform of the time evolution of the coherence, ρ_{01} in the weakly driven case, showing a strong peak at the transition frequency (f_3). (d) Fourier transforms of ρ_{01} with an increasing driving amplitude. The satellite peaks corresponding to $f_3 \pm \Delta$ become clearly visible and shift linearly with the driving amplitude as shown in (e). (f) Energy level scheme of the dressed spin, without (left) and with state dressing (right). Note that here $\Delta = \Omega$, the same as the experimental splitting measured via a second spin.

The time evolution of the off-diagonal elements incorporates the coherence of the system, i.e. the correlations between the states $|0\rangle$ and $|1\rangle$, as well as the Larmor precession. When the spin is coupled with a driving field, in addition, the off-diagonal elements become modulated by the Rabi coupling since the system eigenstates transform into the dressed states $|D\rangle_{\pm}$, which are superpositions of the unperturbed eigenstates, $|0\rangle$ and $|1\rangle$. The coherence element ρ_{01} at $V_{\mathrm{RF2}} = 20$ mV also slowly decayed towards a steady state, with dense oscillations due to the very fast Larmor precession at the transition frequency. To show the frequency spectrum of the signal we took the Fourier transform of the time evolution of ρ_{01} (Fig. 5c). It shows a strong central peak at the transition frequency of spin 2 (f_3) and two weak satellites. The separation between these peaks is too small, and as a consequence, the state dressing in a weakly driven system was not observed in the experiments. In contrast, the Fourier transform of ρ_{01} at $V_{\mathrm{RF2}} = 140$ mV (Fig. 5d) shows two clearly separated satellite peaks, with the separation being linearly dependent on the driving amplitude (see Fig. 5e). We note that in the experiment the splitting between two peaks (α, β) is given by Ω since the transition is probed by a third level which is not dressed (see also Fig. 1d). Similarly, the two side band peaks observed in the density matrix are split by $\pm\Omega$ from the center

frequency, as illustrated in Fig. 5f. The simulations shown here strongly suggest that our designed, weakly coupled two-spin system, combined with the double resonance scheme, can in good approximation be treated as a single dressed two-level system when one of the two spins is strongly driven (see also Fig. S8).

Conclusions

We demonstrated that dressing spin states of an individual atom with resonant RF fields is easily achievable in an ESR-STM at moderate RF voltages owing to the inherently strong electric field in the sub-nm geometry of the STM junction. By utilizing two coupled spins and continuous wave RF excitations at two or three frequencies simultaneously, we measured Autler-Townes doublets and Mollow triplets in the double resonance spectra. From the splitting of the doublet and triplet, we were able to determine the Rabi rate of each spin independently. We anticipate that the techniques shown here are critical for creating decoherence-free subspaces with long-lived quantum states on surfaces. Together with implementation of pulsed multi-resonance ESR with a wide frequency range, the dressed quantum states demonstrated in this work might drive the atomic-scale qubit platform to move towards real implementation of quantum algorithms.

Methods

We performed experiments in an ultra-high vacuum ($P_{base} < 10^{-10}$ mbar) low temperature STM at base temperature of 0.4 K (USM1300, Unisoku), equipped with ^{3}He cryogenics, two-axis superconducting magnets, and RF-compatible signal cables. The sample preparation procedures are described in detail elsewhere[22, 31]. Fe and Ti atoms were deposited on an atomically flat surface of 2 ML-thick MgO on Ag(100) substrate, which is pre-cooled at the STM stage. All measurements were performed on Ti atoms at bridge sites of the MgO surface (that is, in the middle of two oxygen sites). The STM tip was made by mechanical cutting of a Pt/It wire, and its apex was spin-polarized by picking up Fe atoms. Its spin polarization was checked using the asymmetry of the differential conductance ($\mathrm{d}I/\mathrm{d}V$) measured on Ti atoms. The double resonance spectroscopy was performed by applying a RF voltage of two frequencies from the output signals of two RF generators (Agilent E8257D and E8267D) using a power combiner before combining with a DC bias voltage through a bias tee. To read out the spin-polarized current in ESR of the spins, we used a lock-in amplifier (SR860, Stanford Research). The RF signals were chopped at 95 Hz, and this chopper signal was sent to the lock-in amplifier as a reference. The bias voltage refers to the sample voltage relative to the tip. Open quantum systems simulations were performed using the QuTiP package[39] with the Hamiltonian for two-coupled spins and collapse operators as described in our previous work[22].

ACKNOWLEDGMENTS

This work was supported by the Institute for Basic Science (IBS-R027-D1). M.H. acknowledges financial support from University of Tokyo Global Activity Support Program for Young Researchers (FY2020).

ASSOCIATED CONTENT

Supporting Information. The Supporting Information includes a theoretical description of the dressed atom model, additional experimental spectra, temperature logs, and details of open quantum systems simulations. The Supporting Information is available free of charge.

Preprint version. Bui, H. T.; Wolf, C.; Wang, Y.; Haze, M.; Ardavan, A.; Heinrich, A. J.; Phark, S. All-electrical driving and probing of dressed states in a single spin. **2024**, *arXiv*:2401.15440v1. https://doi.org/10.48550/arXiv.2401.15440 (Jan 27, 2024).

AUTHOR INFORMATION

Corresponding Author

*Andreas J. Heinrich (heinrich.andreas@qns.science), Soo-hyon Phark (phark@qns.science)

Author Contributions

A.J.H., C.W., and S.P. conceived the experiment. H.T.B., M.H., Y.W., and S.P. performed experiments and data analysis. C.W. carried out open quantum system simulations. All authors discussed the results and prepared the manuscript together. ‡These authors contributed equally.

REFERENCES

(1) Heinrich, A. J.; Oliver, W. D.; Vandersypen, L. M.; Ardavan, A.; Sessoli, R.; Loss, D.; Jayich, A. B.; Fernandez-Rossier, J.; Laucht, A.; Morello, A. Quantum-coherent nanoscience. *Nature nanotechnology* **2021**, *16* (12), 1318-1329.

(2) Jones, J. A.; Jaksch, D. *Quantum information, computation and communication*; Cambridge University Press, 2012.

(3) Autler, S. H.; Townes, C. H. Stark Effect in Rapidly Varying Fields. *Physical Review* **1955**, *100* (2), 703-722. DOI: 10.1103/PhysRev.100.703.

(4) Miao, K. C.; Blanton, J. P.; Anderson, C. P.; Bourassa, A.; Crook, A. L.; Wolfowicz, G.; Abe, H.; Ohshima, T.; Awschalom, D. D. Universal coherence protection in a solid-state spin qubit. *Science* **2020**, *369* (6510), 1493-1497.

(5) Lynn, T. W. *Measurement and control of individual quanta in cavity QED*; PhD thesis, California Institute of Technology, 2003.

(6) Schabert, A.; Keil, R.; Toschek, P. Dynamic stark effect of an optical line observed by cross-saturated absorption. *Applied physics* **1975**, *6*, 181-184.

(7) Mollow, B. Power spectrum of light scattered by two-level systems. *Physical Review* **1969**, *188* (5).

(8) Wu, F.; Grove, R.; Ezekiel, S. Investigation of the spectrum of resonance fluorescence induced by a monochromatic field. *Physical Review Letters* **1975**, *35* (21), 1426.

(9) Cahuzac, P.; Vetter, R. Observation of the Autler-Townes effect on infrared laser transitions of xenon. *Physical Review A* **1976**, *14* (1), 270.

(10) Gray, H.; Stroud Jr, C. Autler-Townes effect in double optical resonance. *Optics Communications* **1978**, *25* (3), 359-362.

(11) Hao, L.; Jiao, Y.; Xue, Y.; Han, X.; Bai, S.; Zhao, J.; Raithel, G. Transition from electromagnetically induced transparency to Autler–Townes splitting in cold cesium atoms. *New Journal of Physics* **2018**, *20* (7), 073024.

(12) Schmidt, J.; Winnerl, S.; Dimakis, E.; Hübner, R.; Schneider, H.; Helm, M. All-THz pump-probe spectroscopy of the intersubband AC-Stark effect in a wide GaAs quantum well. *Optics Express* **2020**, *28* (17), 25358-25370.

(13) Wrigge, G.; Gerhardt, I.; Hwang, J.; Zumofen, G.; Sandoghdar, V. Efficient coupling of photons to a single molecule and the observation of its resonance fluorescence. *nature physics* **2008**, *4* (1), 60-66.

(14) Xu, X.; Sun, B.; Berman, P. R.; Steel, D. G.; Bracker, A. S.; Gammon, D.; Sham, L. J. Coherent optical spectroscopy of a strongly driven quantum dot. *Science* **2007**, *317* (5840), 929-932.

(15) Muller, A.; Fang, W.; Lawall, J.; Solomon, G. S. Phys. Rev. Lett. *Phys. Rev. Lett* **2008**, *101* (027401).

(16) Flagg, E. B.; Muller, A.; Robertson, J.; Founta, S.; Deppe, D.; Xiao, M.; Ma, W.; Salamo, G.; Shih, C.-K. Resonantly driven coherent oscillations in a solid-state quantum emitter. *Nature Physics* **2009**, *5* (3), 203-207.

(17) Laucht, A.; Kalra, R.; Simmons, S.; Dehollain, J. P.; Muhonen, J. T.; Mohiyaddin, F. A.; Freer, S.; Hudson, F. E.; Itoh, K. M.; Jamieson, D. N. A dressed spin qubit in silicon. *Nature nanotechnology* **2017**, *12* (1), 61-66.

(18) Hargart, F.; Roy-Choudhury, K.; John, T.; Portalupi, S.; Schneider, C.; Höfling, S.; Kamp, M.; Hughes, S.; Michler, P. Probing different regimes of strong field light–matter interaction with semiconductor quantum dots and few cavity photons. *New Journal of Physics* **2016**, *18* (12), 123031.

(19) Viennot, J.; Dartiailh, M.; Cottet, A.; Kontos, T. Coherent coupling of a single spin to microwave cavity photons. *Science* **2015**, *349* (6246), 408-411.

(20) Binnig, G.; Rohrer, H. Scanning tunneling microscopy. *Surface science* **1983**, *126* (1-3), 236-244.

(21) Chen, C. J. *Introduction to Scanning Tunneling Microscopy Third Edition*; Oxford University Press, USA, 2021.

(22) Phark, S.; Chen, Y.; Bui, H. T.; Wang, Y.; Haze, M.; Kim, J.; Bae, Y.; Heinrich, A. J.; Wolf, C. Double-Resonance Spectroscopy of Coupled Electron Spins on a Surface. *ACS nano* **2023**, *17* (14), 14144-14151.

(23) Wang, Y.; Chen, Y.; Bui, H. T.; Wolf, C.; Haze, M.; Mier, C.; Kim, J.; Choi, D.-J.; Lutz, C. P.; Bae, Y. An atomic-scale multi-qubit platform. *Science* **2023**, *382* (6666), 87-92.

(24) Choi, T.; Paul, W.; Rolf-Pissarczyk, S.; Macdonald, A. J.; Natterer, F. D.; Yang, K.; Willke, P.; Lutz, C. P.; Heinrich, A. J. Atomic-scale sensing of the magnetic dipolar field from single atoms. *Nature nanotechnology* **2017**, *12* (5), 420-424.

(25) Baumann, S.; Paul, W.; Choi, T.; Lutz, C. P.; Ardavan, A.; Heinrich, A. J. Electron paramagnetic resonance of individual atoms on a surface. *Science* **2015**, *350* (6259), 417-420.

(26) Willke, P.; Paul, W.; Natterer, F. D.; Yang, K.; Bae, Y.; Choi, T.; Fernández-Rossier, J.; Heinrich, A. J.; Lutz, C. P. Probing quantum coherence in single-atom electron spin resonance. *Science Advances* **2018**, *4* (2), eaaq1543.

(27) Kim, J.; Jang, W.-j.; Bui, T. H.; Choi, D.-J.; Wolf, C.; Delgado, F.; Chen, Y.; Krylov, D.; Lee, S.; Yoon, S.; et al. Spin resonance amplitude and frequency of a single atom on a surface in a vector magnetic field. *Physical Review B* **2021**, *104* (17). DOI: 10.1103/PhysRevB.104.174408.

(28) Reina-Gálvez, J.; Wolf, C.; Lorente, N. Many-body nonequilibrium effects in all-electric electron spin resonance. *Physical Review B* **2023**, *107* (23), 235404.

(29) Bae, Y.; Yang, K.; Willke, P.; Choi, T.; Heinrich, A. J.; Lutz, C. P. Enhanced quantum coherence in exchange coupled spins via singlet-triplet transitions. *Science advances* **2018**, *4* (11), eaau4159.

(30) Yang, K.; Bae, Y.; Paul, W.; Natterer, F. D.; Willke, P.; Lado, J. L.; Ferrón, A.; Choi, T.; Fernández-Rossier, J.; Heinrich, A. J. Engineering the eigenstates of coupled spin-1/2 atoms on a surface. *Physical Review Letters* **2017**, *119* (22), 227206.

(31) Phark, S.; Bui, H. T.; Ferrón, A.; Fernández-Rossier, J.; Reina-Gálvez, J.; Wolf, C.; Wang, Y.; Yang, K.; Heinrich, A. J.; Lutz, C. P. Electric-Field-Driven Spin Resonance by On-Surface Exchange Coupling to a Single-Atom Magnet. *Advanced Science* **2023**, *10* (27), 2302033.

(32) Wang, Y.; Haze, M.; Bui, H. T.; Soe, W.-h.; Aubin, H.; Ardavan, A.; Heinrich, A. J.; Phark, S.-h. Universal quantum control of an atomic spin qubit on a surface. *npj Quantum Information* **2023**, *9* (1), 48.

(33) Yang, K.; Paul, W.; Phark, S.-H.; Willke, P.; Bae, Y.; Choi, T.; Esat, T.; Ardavan, A.; Heinrich, A. J.; Lutz, C. P. Coherent spin manipulation of individual atoms on a surface. *Science* **2019**, *366* (6464), 509-512.

(34) Manzano, D. A short introduction to the Lindblad master equation. *Aip Advances* **2020**, *10* (2), 025106.

(35) Jäck, B.; Eltschka, M.; Assig, M.; Hardock, A.; Etzkorn, M.; Ast, C. R.; Kern, K. A nanoscale gigahertz source realized with Josephson scanning tunneling microscopy. *Applied Physics Letters* **2015**, *106* (1).

(36) Bina, M. The coherent interaction between matter and radiation. *The European Physical Journal Special Topics* **2012**, *203* (1), 163-183.

(37) Larson, J.; Mavrogordatos, T. K. The Jaynes-Cummings model and its descendants. *arXiv preprint arXiv:2202.00330* **2022**.

(38) Baur, M.; Filipp, S.; Bianchetti, R.; Fink, J.; Göppl, M.; Steffen, L.; Leek, P. J.; Blais, A.; Wallraff, A. Measurement of Autler-Townes and Mollow transitions in a strongly driven superconducting qubit. *Physical review letters* **2009**, *102* (24), 243602.

(39) Johansson, J.; Nation, P.; Nori, F. QuTiP 2: A Python framework for the dynamics of open quantum systems. *Computer Physics Communications* **2013**, *4* (184), 1234-1240.

SUPPORTING INFORMATION

All-electrical driving and probing of dressed states in a single spin

Hong T. Bui[1,2‡], *Christoph Wolf*[1,3‡], *Yu Wang*[1,3], *Masahiro Haze*[4], *Arzhang Ardavan*[5], *Andreas J. Heinrich*[1,2*], *Soo-hyon Phark*[1,3*]

[1]Center for Quantum Nanoscience, Institute for Basic Science (IBS), Seoul 03760, Korea

[2]Department of Physics, Ewha Womans University, Seoul 03760, Korea

[3]Ewha Womans University, Seoul 03760, Korea

[4]The Institute for Solid State Physics, University of Tokyo, Kashiwa 277-8581, Japan

[5]CAESR, Clarendon Laboratory, Department of Physics, University of Oxford, Oxford OX1 3PU, UK

Corresponding Author: Andreas J. Heinrich (heinrich.andreas@qns.science), Soo-hyon Phark (phark@qns.science)

Supplementary 1: AC Stark effect in double resonance spectra

In this work, we demonstrated the AC Stark effect in a single spin coupled with a radio-frequency electric field in STM tunnel junction. An elegant approach to understand the AC Stark effect is the "dressed atom" theory as follows. Consider a quantum system of two atom levels, $|0\rangle$ and $|1\rangle$ ($E_{|0\rangle} < E_{|1\rangle}$), in a near-resonant electromagnetic field with photon energy $\hbar\omega$, so that $E_{|1\rangle} - E_{|0\rangle} \approx \hbar\omega$. If photons do not interact with the atom states, the total Hamiltonian is $\hat{H}_0 = \hat{H}_{\text{atom}} + \hat{H}_{\text{field}}$, and the eigenstates of $\hat{H}_0$ are $|0, n\rangle$ and $|1, n\rangle$ where n labels the photon occupation. We notice that the state of the atom level $|1\rangle$ with the photon number $n-1$ ($|1, n-1\rangle$) is almost degenerate with the state $|0, n\rangle$, and so are $|1, n\rangle$ and

$|0, n+1\rangle$. We define the detuning as $\Delta = E_{|1,n-1\rangle} - E_{|0,n\rangle}$, and the two states $|0, n\rangle$ and $|1, n-1\rangle$ become fully degenerate at $\Delta = 0$.

Now if we turn on an interaction $\widehat{H}_{\text{int}}$ between atom and field, the states $|0, n\rangle$ and $|1, n-1\rangle$ become hybridized and their degeneracy lifted. Then, the eigenstates of the system can be described by a linear combination of the two nearly degenerate states of the non-interacting Hamiltonian

$$|D\rangle = C_0|0, n\rangle + C_1|1, n-1\rangle, \quad \text{(Eq. S1)}$$

where the coefficients are obtained from the Schrodinger equation,

$$(\widehat{H}_{\text{atom}} + \widehat{H}_{\text{field}} + \widehat{H}_{\text{int}})|D\rangle = E_{\text{D}}|D\rangle. \quad \text{(Eq. S2)}$$

Defining the Rabi rate as $\hbar\Omega \equiv \langle 1, n-1|\widehat{H}_{\text{int}}|0, n\rangle$, we can solve the secular equation and obtain the eigenenergies

$$E_{\text{D}} = (n - 1/2)\hbar\omega \pm \hbar\Omega_{\text{R}}/2, \quad \Omega_{\text{R}} = \sqrt{\Delta^2 + \Omega^2}, \quad \text{(Eq. S3)}$$

and the corresponding eigenstates,

$$|D(n)\rangle_+ = \sin\theta\,|0, n\rangle + \cos\theta\,|1, n-1\rangle, \quad \text{(Eq. S4)}$$

$$|D(n)\rangle_- = \cos\theta\,|0, n\rangle - \sin\theta\,|1, n-1\rangle, \quad \text{(Eq. S5)}$$

where $\cos 2\theta \equiv \Delta/\Omega_{\text{R}}$ and $\sin 2\theta \equiv \Omega/\Omega_{\text{R}}$. At resonance ($\Delta = 0$), $\sin\theta = \cos\theta = 1/\sqrt{2}$, and the new eigenstates are split by the Rabi rate Ω due to the atom-field interaction $\widehat{H}_{\text{int}}$.

In our double resonance experiment, four spin states are involved. However, in each experiment, only one ESR transition was strongly driven. For example, only the transition f_1 between states $|00\rangle$ and $|10\rangle$ as shown in Fig. 2b. As a result, the ESR transition between the states $|00\rangle$ and $|01\rangle$ occurs at two distinct frequencies $f_3^{(\pm)} = f_3 \pm \Omega^{(1)}/2$ when probed by another weak electromagnetic field that was swept across the Ti-2 resonance f_3. The splitting allows us to determine the Rabi rate of Ti-1 as $\Omega^{(1)}/(2\pi V_{\text{RF1}}) = 0.160 \pm 0.015$ MHz/mV (Fig. 2c). The ESR peak heights at $f_3^{(\pm)}$ are sensitive to the detuning Δ due to its influence on the coefficients $\sin\theta$ and $\cos\theta$ in Eqs. S4 and S5, which is also seen in our simulations in Fig. S5. We omit the quantum numbers of the photon states for convenience in the main figures and text.

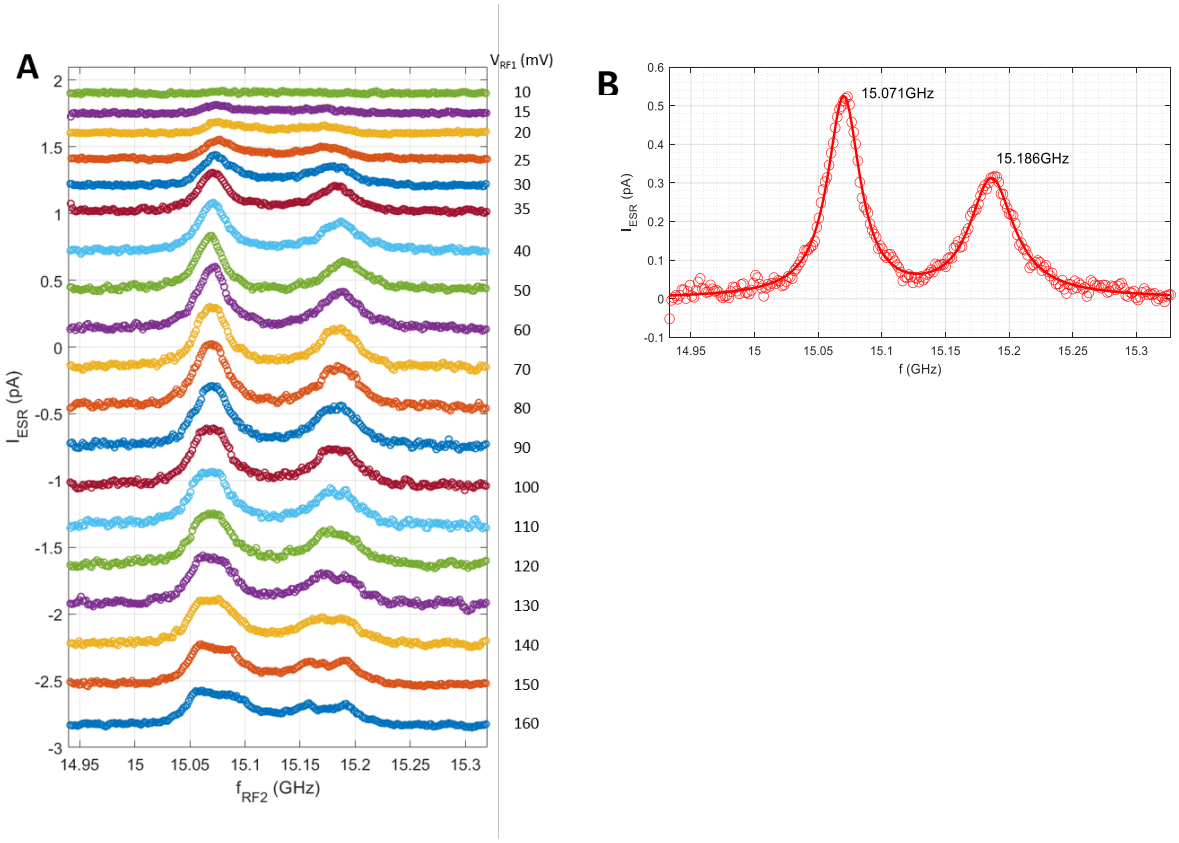

Figure S1. Complete set of double resonance spectra across the two resonances of Ti-2, f_3 and f_4. (A) double resonance spectra measured with f_{RF1} fixed at $f_1 = 16.289$ GHz over a wide range of V_{RF1} ($I_{\mathrm{DC}} = 20$ pA, $V_{\mathrm{DC}} = 50$ mV, $V_{\mathrm{RF2}} = 30$ mV, $0.4 < T < 0.5$ K). (B) 2-Lorentzian curve fit to double resonance spectrum at $V_{\mathrm{RF1}} = 60$ mV, yielding the resonance frequencies of Ti-2 spin, f_3 and f_4, in the absence of the tip's magnetic field.

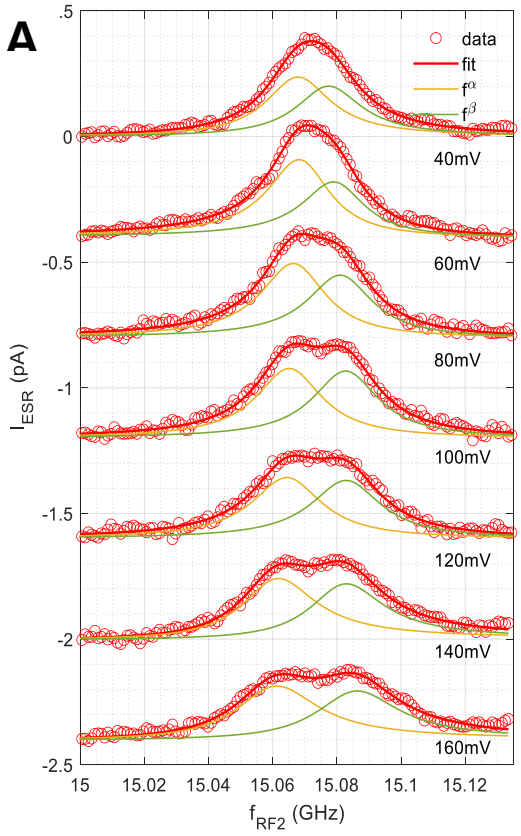

B

V_{RF1}(mV)	fα (GHz)	fβ (GHz)	$\Delta f^{\alpha\beta}$(MHz)
40	15.068	15.077	9.569
60	15.069	15.080	10.782
80	15.067	15.081	14.570
100	15.065	15.083	17.578
120	15.065	15.083	18.427
140	15.064	15.085	21.177
160	15.063	15.088	25.055

Figure S2. Fitting of double resonance peak splitting in Fig. 2a. (A) 2-Lorentzian curve fits to double resonance spectra in Fig. 2a. For each curve, the two peaks were fitted with one common peak width and two independent peak heights. (B) Peak frequencies (f_3^{α}, f_3^{β}) and splitting $\Delta f^{\alpha\beta} = f_3^{\beta} - f_3^{\alpha}$, extracted from the fits in A.

Supplementary 2: The influence of tip height on dressing Ti-1

To characterize the influence of tip-induced field on the ESR driving strength of a spin under the tip, we performed single and double resonance experiments with a varying tip height, which is adjusted by tunneling current and/or DC bias voltage, as shown in Fig. S3.

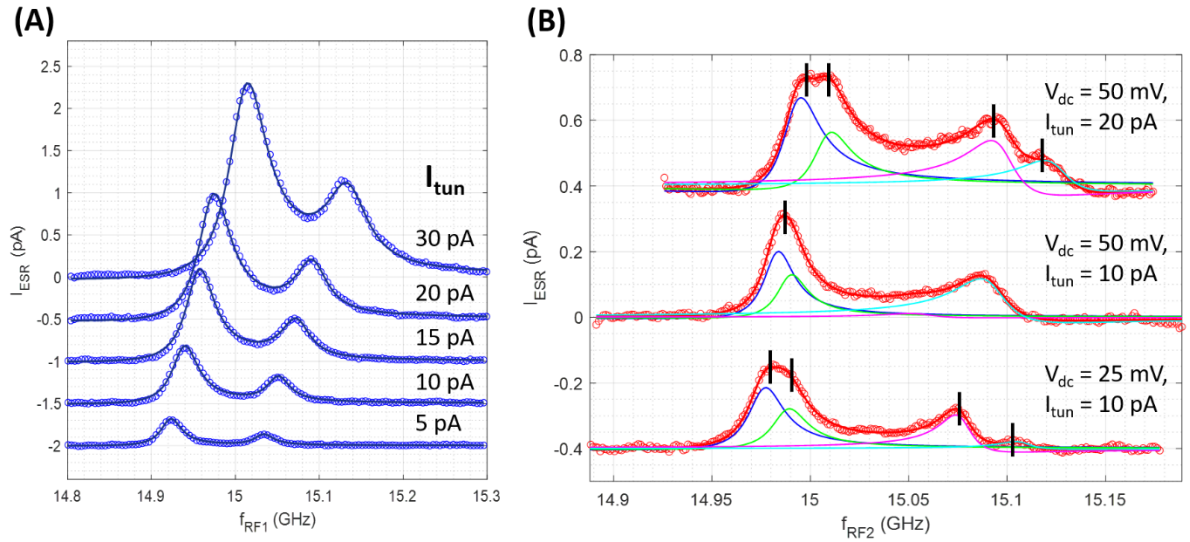

Figure S3. Autler-Townes doublets of Ti-1 at different tip heights. (**A**) Ti-1 ESR spectra obtained from the third spin-polarized tip with the increase of tunneling current from 5 to 30 pA at the constant bias voltage V_{DC} = 50 mV, indicating a closer tip-atom distance. The shift of ESR frequency is caused by the change in the contribution of B_{tip} to the total Zeeman energy. The significant increase in peak amplitude illustrates the enhancement of driving RF electric field. (**B**) Double resonance spectra of Ti-2 spin at three different tunneling conditions but the same RF voltage. The top and bottom curves were obtained at the same tunneling conductance G = 0.4 nS, generated by changing both bias voltage and current as denoted in the figure legend, while the middle one was measured at G = 0.2 nS, i.e., the tip is farer compared to the other two cases. We note that the change in tip height can have additional effects on the effective field strength enhancement in the junction which does not need to be linear (see Figure S8). The spectrum at the top shows splitting of both peaks, an evidence of AC Stack effect, which is similar to the one appeared in the spectrum at the bottom, clearly indicating that the same tip-atom distances generate an identical driving strength. It is worth reminding that the driving of the remote spin is irrelevant to the tunneling current, therefore, the peak amplitudes in all 3 spectra do not show a dramatic change. On the contrary, AT doublets are not clearly resolved in the spectrum in the middle, indicative of a weaker driving strength when the tip is retracted. ($V_{RF2} = 30$ mV, $T = 0.4$ K, $B_{ext} = 610$ mT, $\theta_{ext} = 100^{\circ}$).

Supplementary 3: Autler-Townes doublets from dressing Ti-2

We also observed Autler-Townes doublets by dressing Ti-2 at different vector magnetic fields and tips. Figures S4A-C show the splitting of Ti-1 transitions with varying RF driving voltages on Ti-2, obtained using the same tip but at three different $\boldsymbol{B}_{\mathrm{ext}}$, which resulted in different Rabi rates as shown in Figs. S4E-G, respectively. The change of $\boldsymbol{B}_{\mathrm{ext}}$ changed the interaction between the spins of Ti-2 and Fe, leading to that in the spin-field coupling of Ti-2, which results in the change in the Rabi rate [1]. We found that shape of a tip can lead to a considerable influence on the AT doublets. Figures S4D and H show the spectra and extracted Rabi rate measured using the tip for the data in Fig. 4 of the main text, showing a Rabi rate larger by a factor of ~2 compared to that from the tip for Figs. S4A-C. We attribute such an increase of Rabi rate to that of the RF electric field due to the difference in the shape of the tip body, which can lead to a substantial difference in the spin-field coupling to Ti-2. In addition, we note in this case that the AT doublets are resolved at the driving voltage V_{RF2} from around 30 mV. Together with the AT doublets resolvable at V_{RF2} from around 50 mV using the first tip (Figs. S4 E, F, G), this may imply the dependence of the threshold of the RF voltage for AT doublets to be resolved in our double resonance spectra on the spin-field coupling, which is strongly influenced by the specific shape of the tip. To obtain the resonance frequencies of the four transitions shown in Figs. 3 and 4, we performed single- and dual-frequency ESR at relatively low RF voltages. Figure S5 shows single and double resonance spectra with experimental conditions used for the data in Figs. 3 (A and B) and 4 (C and D) (see figure captions).

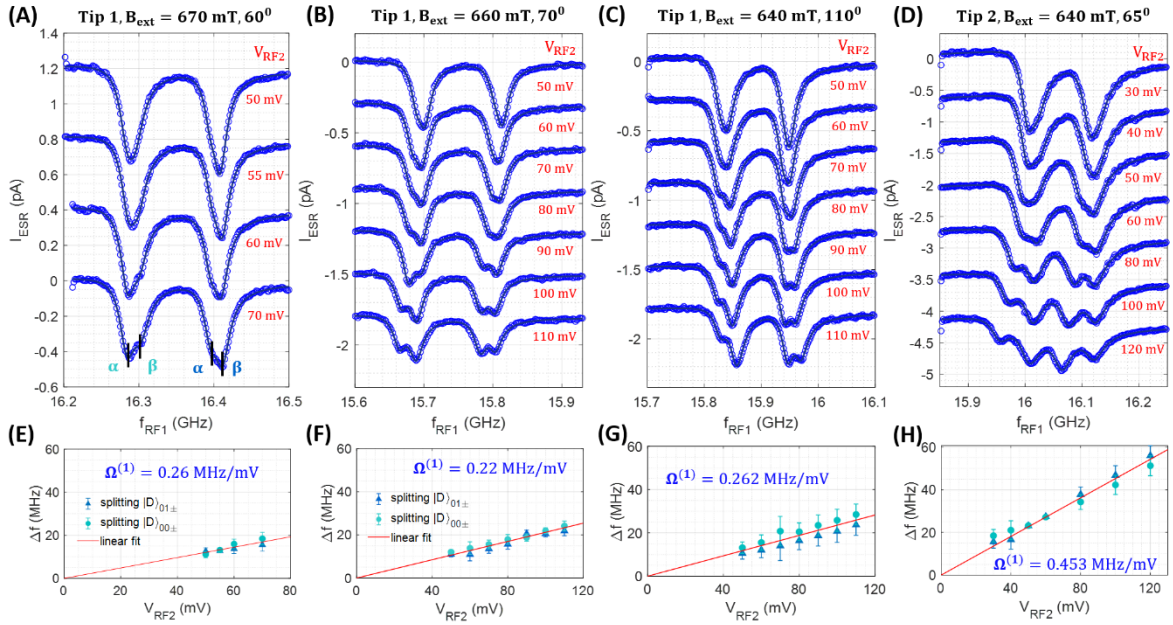

Figure S4. Autler-Townes doublets probed using the transitions of Ti-1. (A-D) Series of ESR spectra of AT doublets measured on Ti-1 for varying V_{RF2}s obtained using the tip for the data shown in Figs. 2 and 3 (A, B, and C) and another tip for the data in Fig. 4 (D). Solid curves overlayed on the data are 4-Lorentzian curve fits to each spectrum. For each curve, the two subpeaks were fitted with one common peak width and two independent peak heights. All measurements were performed at $I_{\mathrm{DC}} = 20$ pA, $V_{\mathrm{DC}} = 50$ mV, $V_{\mathrm{RF1}} = 30$ mV, $T = 0.4$ K. (E-H) Dependence of the splitting of the AT doublets on V_{RF2} extracted from the spectra in A-D, respectively. From the linear fits, we derived the Rabi rates of the remote spin (Ti-2) as denoted in each panel.

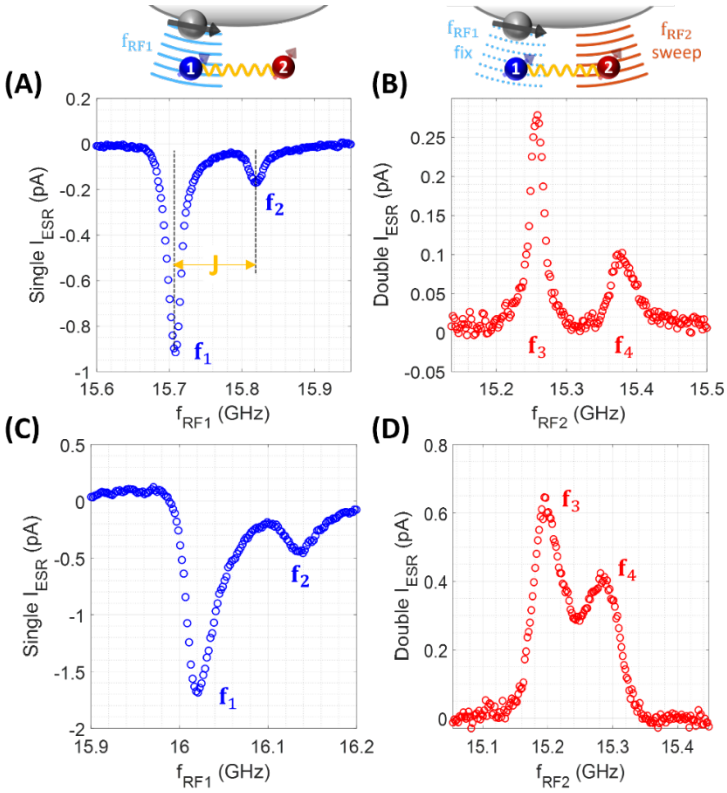

Figure S5. Representative ESR spectra for the data in Figs. 3 and 4. (**A** and **B**) Spectra from single resonance ESR on Ti-1 and double resonance ESR on Ti-2 using the same tip and at the same measurement conditions for the data in Fig. 3. (**C** and **D**) Spectra from single resonance ESR on Ti-1 and double resonance ESR on Ti-2 using the same tip and at the same measurement conditions for the data in Fig. 4. All spectra were measured at $I_{\mathrm{DC}} = 20$ pA, $V_{\mathrm{DC}} = 50$ mV, $V_{\mathrm{RF1}} = 30$ mV, $V_{\mathrm{RF2}} = 30$ mV, $T = 0.4$ K.

Supplementary 4: Temperature effect

Application of RF bias voltage to the STM junction indeed causes local heating. We recorded resultant changes of sample temperature during all the measurements reported in this article. For example, we show the temperature log recorded at a varying RF voltage during the double resonance experiments shown in Fig. 2 (Figs. S6A and B). In addition, thermal spin populations of the four states calculated using the sample temperature for each RF voltage are shown (Fig. S6C).

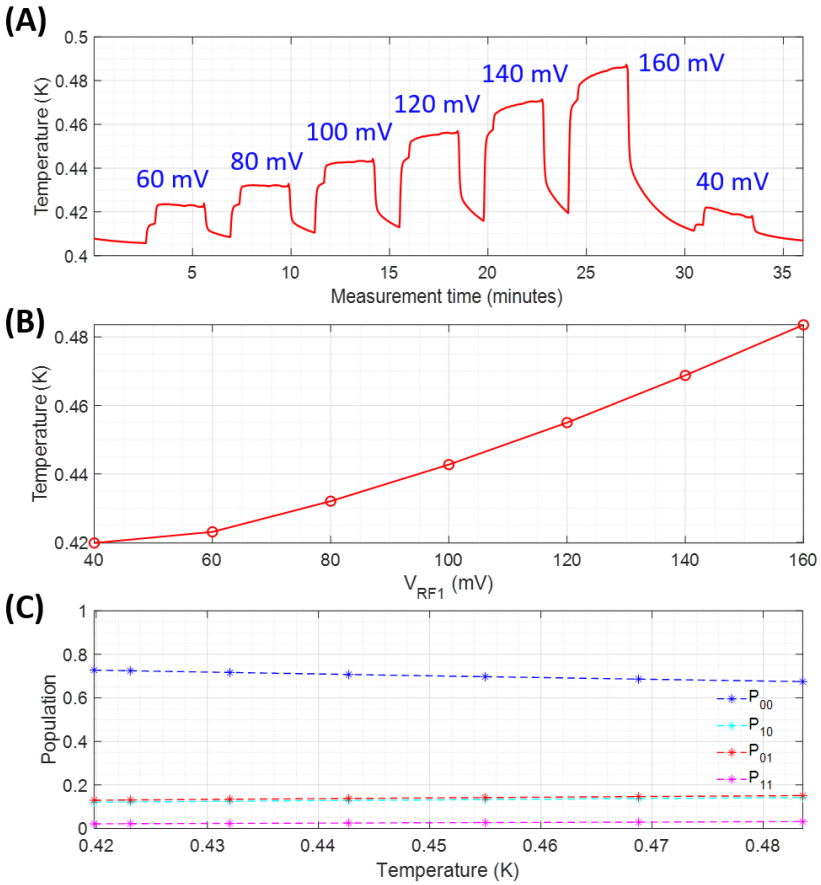

Figure S6. Effect of temperature in double resonance experiment. (**A**) The sample temperature recorded during the double resonance spectroscopy shown in Fig. 2, reflecting the heating effect from the RF power. (**B**) The dependence of the temperature on V_{RF1}. Each data point represents the average temperature over the time for the RF power switched on for each measurement. (**C**) The estimation of the spin populations of the four eigenstates in thermal equilibrium as a function of the temperature shown in B.

Supplementary 5: Detuning effect

A small detuning ($\delta \equiv f_{\mathrm{RF}} - f_{\mathrm{res}} < 10$ MHz) can change the relative peak heights of the Autler-Townes doublets as shown in Fig. S7. Such detuning can occur in the experiment due to imperfect frequency tuning in the RF generator or external magnetic field fluctuations.

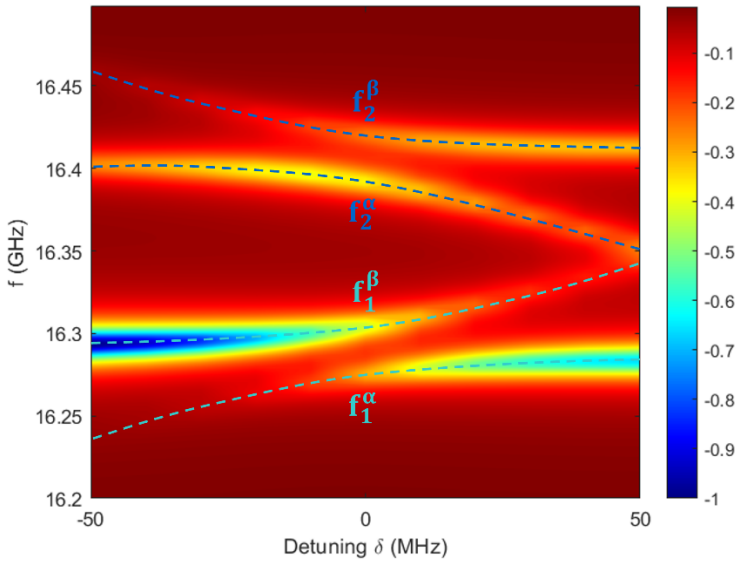

Figure S7. Effect of detuning of the ESR driving on simulated spectra. Simulated Ti-1 double resonance spectra for varying detuning δ of f_{RF2} for $V_{\mathrm{RF2}} = 70$ mV, $T_1^{(1)} = 8$ ns, $T_1^{(2)} = 150$ ns at the magnetic field used in Fig. 1. Vertical lines correspond to the sub-peaks of the spectrum.

Supplementary 6: Dressed density matrix

To obtain the frequency decomposition of the density matrix we first calculated the reduced density matrix of the dressed spin by tracing out the first spin, i.e., $\rho^{(2)} = \mathrm{Tr}_1[\rho]$, where the superscript denotes the spin. The resulting 2×2 density matrix of the dressed spin reads the Eq. (1)

$$\rho^{(2)} = \begin{bmatrix} \rho_{00} & \rho_{01} \\ \rho_{10} & \rho_{11} \end{bmatrix}, \tag{1}$$

which is composed of 4 components representing the spin dynamics only for the second spin (Ti-2), two for its populations $\rho_{00} = p_0^{(2)}$, $\rho_{11} = p_1^{(2)}$ on the diagonals and the other two for its coherences ρ_{01}, ρ_{10} on the off-diagonals. The spectra in Figs. 5c and 5d were obtained by numerical Fourier transformation of the off-diagonal element ρ_{01}. We note that taking the trace is not a strict requirement as it does not change the frequencies present in the Fourier transform and only slightly modifies the amplitudes, see Fig. S8.

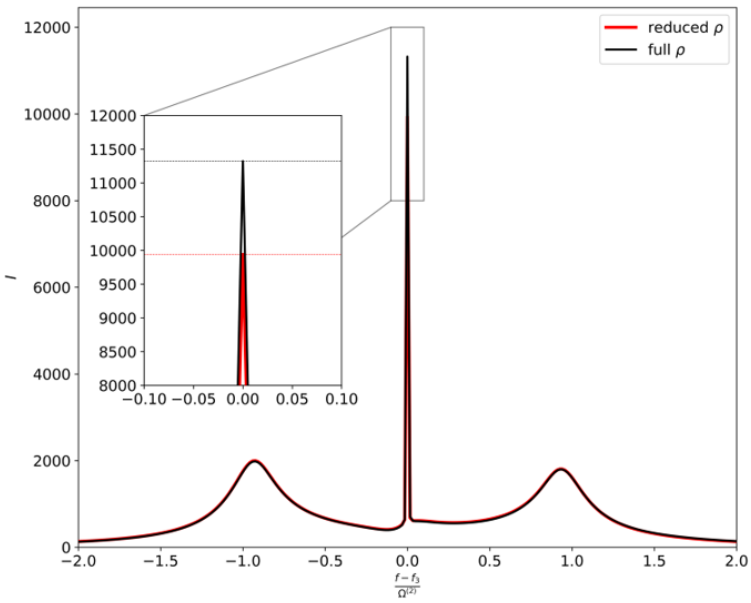

Figure S8. Frequency spectrum for a strongly driven (V_{RF2} = 140 mV) spin obtained from the relevant off-diagonal element of the full (black) and reduced (red) density matrix. In both cases the splitting is clearly visible and identical, but the intensity of the center peak is slightly reduced in the Fourier transform of the reduced density matrix as shown in the inset.

Supplementary 7: Simulation of electric field in STM junction

Enhancement of the electro-magnetic field in the STM nanocavity[2] obtained from FDTD simulations using Ansys.

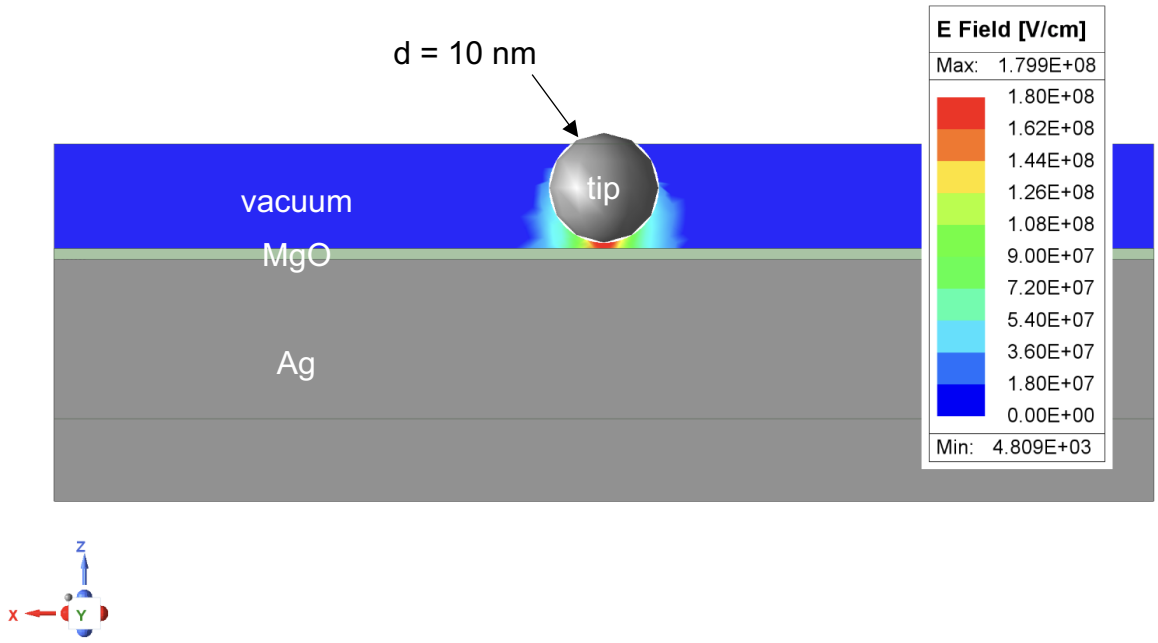

Figure S9: simplified model of an STM junction. The STM tip is represented by a silver sphere of diameter 10 nm and the substrate is represented by a thick slab of silver capped with a dielectric corresponding to 2 monolayers of MgO. The field enhancement in the junction can reach 4×10^4 compared to a plate capacitor model.

REFERENCES:

(1) Phark, S.; Bui, H. T.; Ferrón, A.; Fernández-Rossier, J.; Reina-Gálvez, J.; Wolf, C.; Wang, Y.; Yang, K.; Heinrich, A. J.; Lutz, C. P. Electric-Field-Driven Spin Resonance by On-Surface Exchange Coupling to a Single-Atom Magnet. *Advanced Science* **2023**, *10* (27), 2302033.

(2) Ast, C. R.; Kot, P.; Ismail, M.; de-la-Peña, S.; Fernández-Domínguez, A. I.; Cuevas, J. C. Theory of Electron Spin Resonance in Scanning Tunneling Microscopy. *arXiv preprint arXiv:2403.20247* **2024**.